

Collision off-axis position dependence of relativistic nonlinear Thomson inverse scattering of an excited electron in a tightly focused circular polarized laser pulse

Yubo Wang(王禹博), Qingyu Yang(杨青屿), Yifan Chang(常一凡), Zongyi Lin(林宗熠), and Youwei Tian(田友伟)
Citation: Chin. Phys. B, 2024, 33 (**1**): 013301. DOI: 10.1088/1674-1056/acd921
Journal homepage: http://cpb.iphy.ac.cn; http://iopscience.iop.org/cpb

What follows is a list of articles you may be interested in

Generation of quasi-chirp-free isolated attosecond pulses from atoms under the action of orthogonal two-color combined pulse of fundamental frequency and higher intensity second harmonic fields

Rui-Xian Yu(蔚瑞贤), Yue Qiao(乔月), Ping Li(李萍), Jun Wang(王俊), Ji-Gen Chen(陈基根), Wei Feng(冯伟), Fu-Ming Guo(郭福明), and Yu-Jun Yang(杨玉军)
Chin. Phys. B, 2023, 32 (**6**): 063302. DOI: 10.1088/1674-1056/acc80a

High harmonic generation in crystal SiO_2 by sub-10-fs laser pulses

Shuai Wang(王帅), Jiawei Guo(郭嘉为), Xinkui He(贺新奎), Yueying Liang(梁玥瑛), Baichuan Xie(谢百川), Shiyang Zhong(钟诗阳), Hao Teng(滕浩), and Zhiyi Wei(魏志义)
Chin. Phys. B, 2023, 32 (**6**): 063301. DOI: 10.1088/1674-1056/acc452

Attosecond spectroscopy for filming the ultrafast movies of atoms, molecules and solids

Lixin He(何立新), Xiaosong Zhu(祝晓松), Wei Cao(曹伟), Pengfei Lan(兰鹏飞), and Peixiang Lu(陆培祥)
Chin. Phys. B, 2022, 31 (**12**): 123301. DOI: 10.1088/1674-1056/aca6d2

Ultrafast Coulomb explosion imaging of molecules and molecular clusters

Xiaokai Li(李孝开), Xitao Yu(余西涛), Pan Ma(马盼), Xinning Zhao(赵欣宁), Chuncheng Wang(王春成), Sizuo Luo(罗嗣佐), and Dajun Ding(丁大军)
Chin. Phys. B, 2022, 31 (**10**): 103304. DOI: 10.1088/1674-1056/ac89df

Enhancement of isolated attosecond pulse generation by using long gas medium

Yueying Liang(梁玥瑛), Xinkui He(贺新奎), Kun Zhao(赵昆), Hao Teng(滕浩), and Zhiyi Wei(魏志义)
Chin. Phys. B, 2022, 31 (**4**): 043302. DOI: 10.1088/1674-1056/ac29a8

Collision off-axis position dependence of relativistic nonlinear Thomson inverse scattering of an excited electron in a tightly focused circular polarized laser pulse

Yubo Wang(王禹博)[1], Qingyu Yang(杨青屿)[1], Yifan Chang(常一凡)[2], Zongyi Lin(林宗熠)[1], and Youwei Tian(田友伟)[2,†]

[1] *Bell Honors School, Nanjing University of Posts and Telecommunications, Nanjing* 210023, *China*
[2] *College of Science, Nanjing University of Posts and Telecommunications, Nanjing* 210023, *China*

(Received 17 January 2023; revised manuscript received 23 May 2023; accepted manuscript online 26 May 2023)

This paper presents a novel view of the impact of electron collision off-axis positions on the dynamic properties and relativistic nonlinear Thomson inverse scattering of excited electrons within tightly focused, circularly polarized laser pulses of varying intensities. We examine the effects of the transverse ponderomotive force, specifically how the deviation angle and speed of electron motion are affected by the initial off-axis position of the electron and the peak amplitude of the laser pulse. When the laser pulse intensity is low, an increase in the electron's initial off-axis distance results in reduced spatial radiation power, improved collimation, super-continuum phenomena generation, red-shifting of the spectrum's harmonic peak, and significant symmetry in the radiation radial direction. However, in contradiction to conventional understandings, when the laser pulse intensity is relatively high, the properties of the relativistic nonlinear Thomson inverse scattering of the electron deviate from the central axis, changing direction in opposition to the aforementioned effects. After reaching a peak, these properties then shift again, aligning with the previous direction. The complex interplay of these effects suggests a greater nuance and intricacy in the relationship between laser pulse intensity, electron position, and scattering properties than previously thought.

Keywords: relativistic nonlinear Thomson inverse scattering, off-axis collision, radiation angle distribution, tightly focused laser pulse

PACS: 33.20.Xx, 03.50.De, 41.75.Jv, 52.38.Ph **DOI:** 10.1088/1674-1056/acd921

1. Introduction

Recent years have witnessed significant advancement in the study of high-power laser–matter interactions,[1–6] particularly within the field of ultrafast laser physics.[7–10] A notable area of focus within this realm is the investigation of relativistic nonlinear Thomson inverse scattering (RNTIS), an important mechanism behind the modulated generation of high-energy x-rays[11,12] and gamma rays.[13–15] The study of RNTIS not only contributes to the broader understanding of laser–matter interactions but also has far-reaching applications in various disciplines, such as biomedicine,[16,17] atomic physics,[18,19] and laser-constrained nuclear fusion.[20]

RNTIS involves the elastic scattering of photons and electrons, as depicted in Fig. 1. Its nonlinear nature is due to the inclusion of the Doppler shift. Earlier studies have examined various aspects of radiation produced by laser pulses colliding with electrons. Zhuang *et al.*[11] focused on the quasi-monochromatic x-ray spectra generated by the interaction of low-energy electrons and lasers. The work of Taira *et al.*[15,21,22] probed the angular distribution of radiative harmonic energy in RNITS. Significant contributions to understanding the dynamics of tightly focused laser-driven electrons were made by Liu *et al.*[23] Chang *et al.*[24] explored the properties of radiation from tightly focused center colliding RNITS, delving into methods of modulating high-energy gamma rays.

Most previous research primarily investigates the direct collision of electrons with tightly focused laser pulses. However, in practical settings, it is challenging to constrain the electron to the axis along which the laser pulse is located. Consequently, the characteristics of the electron's interaction with the laser under off-axis conditions urgently need exploration and understanding. Yu *et al.*[25] studied the effect of the initial off-axis position of the electron acceleration driven by ponderomotive force in a plane wave laser field. Nonetheless, in the tightly focused Gaussian polarized laser field, the dynamic and nonlinear properties of the electron are significantly influenced by the tight focus characteristics of the strong laser field. Furthermore, the impact of electron off-axis position on space radiation has not been previously investigated.

This paper presents the first-ever study of the dynamic properties, spatial radiated power, and spectral characteristics of electrons under off-axis collision conditions within a circularly polarized, tightly focused laser field. We investigate the effects of the peak amplitude of the laser pulse and the initial off-axis position of the electron on its dynamic properties, the angular spatial distribution of radiated power, the peak power of spatial radiation, and radiation collimation.

The research findings suggest that the trajectory of an ex-

[†]Corresponding author. E-mail: tianyw@njupt.edu.cn

© 2024 Chinese Physical Society and IOP Publishing Ltd

cited electron's motion is influenced by both laser intensity and its initial off-axis position. The electron eventually deviates from the laser pulse's central axis at a constant speed, with the deviation angle's magnitude affected by the laser intensity and the initial off-axis position of the electron. With relatively low-intensity laser pulses, the radiation radial direction shows significant symmetry around $\phi = 0°$. As the electron's initial off-axis distance increases, the spatial radiation peak power decreases, and collimation improves. Additionally, the multimodality of the electron radiation spectrum lessens, supercontinuum phenomena emerge, and the harmonic peak of the radiation spectrum exhibits red-shifts, resulting in a decrease in radiation light intensity. Conversely, under the influence of a relatively high-intensity laser pulse, the spatial radiation power angle distribution of the electron initially increases then decreases as the initial off-axis distance of the electron increases. Similarly, collimation initially weakens and then strengthens. The initial off-axis distance that corresponds to the highest radiation peak power point is identical to that corresponding to the lowest radiation peak angle, under the same laser pulse intensity. The multimodality of the electron radiation spectrum varies in different directions with the change in the electron's initial off-axis distance. The radiation spectrum harmonic peak shows a distinct blue-shift phenomenon in specific directions. However, with a further increase in the electron's initial off-axis distance, the radiation spectrum harmonic peak undergoes a red-shift phenomenon in all directions.

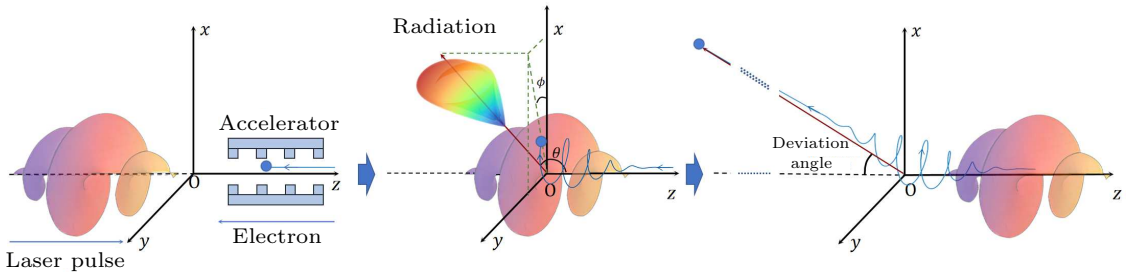


Fig. 1. Schematic diagram of relativistic nonlinear Thomson inverse scattering process.

The remainder of this paper is structured as follows. In Section 2, we derive analytical expressions for the vector potential of the laser pulse, the laws governing electron motion, and the radiation spectrum, using principles of classical electrodynamics. In Section 3, we explore the impact of the peak amplitude of the laser pulse and the initial off-axis position of the electron on the spatial radiation power and radiation spectrum of the electron. Section 4 presents a summary of the effects of the electron's initial off-axis position and the peak amplitude of the laser pulse on electron dynamics, spatial radiation power, and the radiation spectrum. Additionally, we discuss how to modulate radiation rays to achieve desirable monochromaticity, intensity, and high frequency or high collimation by controlling laser intensity and the initial off-axis position of the electron.

2. Theory and formula

To begin, we must note that all subsequent formula definitions have spatial and temporal coordinates normalized by the wave number of the laser, denoted as $k_0^{-1} = \lambda_0/(2\pi)$, and the frequency of the laser, denoted as $\omega_0^{-1} = \lambda_0/(2\pi c)$. Here λ_0 represents the wavelength of the laser, corresponding to 1 μm, c is the speed of light, ε is the dielectric constant, m and e represent the mass and charge of the electron, respectively.

We consider a Laguerre–Gaussian (LG) laser pulse propagating along the z-axis at an angle of incidence $\sigma_{\text{in}} = 0$, and with the dielectric media being isotropic, homogeneous, nonmagnetic, and nonconducting. In a tightly focused Gaussian laser field, the electric field $\boldsymbol{E}$ and magnetic field $\boldsymbol{B}$, satisfying Maxwell's equations, can be expressed as follows:[26,27]

$$\boldsymbol{E} = \boldsymbol{\nabla} \times \boldsymbol{A}, \tag{1}$$

$$\boldsymbol{B} = \sqrt{\varepsilon}\left[\left(\frac{\mathrm{i}}{k}\right)\boldsymbol{\nabla}(\boldsymbol{\nabla}\cdot\boldsymbol{A}) + \mathrm{i}k\boldsymbol{A}\right], \tag{2}$$

where $\boldsymbol{A}$ is the solution to the Helmholtz equation

$$\boldsymbol{\nabla}^2\boldsymbol{A} + k_0^2\boldsymbol{A} = 0. \tag{3}$$

Within the laser field, circularly polarized laser light can be decomposed into a pair of x-axis and y-axis linearly polarized lasers with a phase difference of $\pi/2$. Thus, the electromagnetic field of the circularly polarized laser can also be decomposed similarly, that is, $\boldsymbol{E} = \boldsymbol{E}_{xp} + \boldsymbol{E}_{yp}$, $\boldsymbol{B} = \boldsymbol{B}_{xp} + \boldsymbol{B}_{yp}$. Yousef *et al.*[28] derived $\boldsymbol{A}$, $\boldsymbol{B}$, and $\boldsymbol{E}$ in the x-axis linearly polarized laser field from Eqs. (1)–(3). Zhang[29] and Barton[26] proposed the electromagnetic field expression of the y-axis linearly polarized laser field using symmetry expression. Combining the above, the electric field component $\boldsymbol{E} = \{E_x, E_y, E_z\}$ can be derived as

$$E_x = E_{\text{L}}\left\{S_0 + \varepsilon^2\left[\xi^2 S_2 - \frac{r^4 S_3}{4}\right] + \varepsilon^4\left[\frac{S_2}{8} - \frac{r^2 S_3}{4} - \frac{r^2\left(r^2 - 16\xi^2\right)S_4}{16}\right.\right.$$

$$-\frac{r^4\left(r^2+2\alpha^2\right)S_5}{8}+\frac{r^8S_6}{32}\Bigg]$$
$$+\varepsilon^2C_2+\varepsilon^4\left[r^2C_4-\frac{r^4C_5}{4}\right]\Bigg\}, \tag{4}$$

$$E_y = E_{\rm L}\Bigg\{C_0+\varepsilon^2\left[\beta^2C_2-\frac{r^4C_3}{4}\right]$$
$$+\varepsilon^4\Bigg[\frac{C_2}{8}-\frac{r^2C_3}{4}-\frac{r^2\left(r^2-16\beta^2\right)C_4}{16}$$
$$-\frac{r^4\left(r^2+2\beta^2\right)C_5}{8}+\frac{r^8C_6}{32}\Bigg]$$
$$+\varepsilon^2S_2+\varepsilon^4\left[r^2S_4-\frac{r^4S_5}{4}\right]\Bigg\}, \tag{5}$$

$$E_z = E_{\rm L}\xi\Bigg\{\varepsilon C_1+\varepsilon^3\left[-\frac{C_2}{2}+r^2C_3-\frac{r^4C_4}{4}\right]$$
$$+\varepsilon^5\Bigg[-\frac{3C_3}{8}-\frac{3r^2C_4}{8}+\frac{17r^4C_5}{16}$$
$$-\frac{3r^6C_5}{16}-\frac{3r^6C_6}{8}+\frac{r^8C_7}{32}\Bigg]\Bigg\}$$
$$-K_{\rm L}\beta\Bigg\{\varepsilon S_1+\varepsilon^3\left[-\frac{S_2}{2}+r^2S_3-\frac{r^4S_4}{4}\right]$$
$$+\varepsilon^5\Bigg[-\frac{3S_3}{8}-\frac{3r^2S_4}{8}+\frac{17r^4S_5}{16}$$
$$-\frac{3r^6S_5}{16}-\frac{3r^6S_6}{8}+\frac{r^8S_7}{32}\Bigg]\Bigg\}, \tag{6}$$

and the magnetic field components are described as follows:

$$B_x = E_{\rm L}\Bigg\{C_0+\varepsilon^2\left[\frac{r^2C_2}{2}-\frac{r^4C_3}{4}\right]+\varepsilon^4\Bigg[-\frac{C_2}{8}+\frac{r^2C_3}{4}$$
$$+\frac{5r^4C_4}{16}-\frac{r^6C_5}{4}+\frac{r^8C_6}{32}\Bigg]\Bigg\}, \tag{7}$$

$$B_y = E_{\rm L}\Bigg\{S_0+\varepsilon^2\left[\frac{r^2S_2}{2}-\frac{r^4S_3}{4}\right]+\varepsilon^4\Bigg[-\frac{S_2}{8}+\frac{r^2S_3}{4}$$
$$+\frac{5r^4S_4}{16}-\frac{r^6S_5}{4}+\frac{r^8S_6}{32}\Bigg]\Bigg\}, \tag{8}$$

$$B_z = E_{\rm L}\beta\Bigg\{\varepsilon C_1+\varepsilon^3\left[\frac{C_2}{2}+\frac{r_2C_3}{2}-\frac{r_4C_4}{4}\right]$$
$$+\varepsilon_5\left[\frac{3C_3}{8}+\frac{3r^2C_4}{8}+\frac{3r^4C_5}{16}-\frac{r^6C_6}{4}+\frac{r^8C_7}{32}\right]\Bigg\}$$
$$-E_{\rm L}\xi\Bigg\{\varepsilon S_1+\varepsilon^3\left[\frac{S_2}{2}+\frac{r_2S_3}{2}-\frac{r_4S_4}{4}\right]$$
$$+\varepsilon_5\left[\frac{3S_3}{8}+\frac{3r^2S_4}{8}+\frac{3r^4S_5}{16}-\frac{r^6S_6}{4}+\frac{r^8S_7}{32}\right]\Bigg\}, \tag{9}$$

where $\xi = x/w_0$, $\beta = y/w_0$, $r = \rho/w_0$, w_0 represents the minimum waist radius. The electromagnetic field is fifth-order expanded accurate to the diffraction angle $\varepsilon = w_0/z_{\rm R}$, and $E_{\rm L}$ can be expressed as follows:

$$E_{\rm L} = a_0\frac{w_0}{w}\exp\left[-\frac{\eta^2}{L^2}\right]\exp\left(-\frac{\rho^2}{w^2}\right), \tag{10}$$

where $\eta = z-t$, $w = w_0\sqrt{1+z^2/z_{\rm R}^2}$ represents the waist radius at z, $z_{\rm R} = w_0^2/2$ indicates the Rayleigh distance, $\rho = \sqrt{x^2+y^2}$ denotes the perpendicular distance, and $a_0 = \sqrt{I\lambda_0^2/1.37}\times 10^9$ indicates the peak amplitude.

The electromagnetic field is fifth-order expanded accurate to the diffraction angle $\varepsilon = w_0/z_{\rm R}$, and among them, S_n and C_n are shown as follows:

$$S_n = \left(\frac{w_0}{w}\right)^n\sin\left(\varphi+n\varphi_{\rm G}\right),\ \ n=0,1,2,\ldots, \tag{11}$$

$$C_n = \left(\frac{w_0}{w}\right)^n\cos\left(\varphi+n\varphi_{\rm G}\right),\ \ n=0,1,2,\ldots, \tag{12}$$

where $\varphi = \varphi_0+\eta-\varphi_{\rm R}+\varphi_{\rm G}$, the initial phase φ_0 is the phase of plane wave. The phase related to the curvature of wave fronts $\varphi_{\rm R}$ is defined as $\varphi_{\rm R} = \rho^2/(2R(z))$, and $R(z) = z+z_{\rm R}^2/z$ indicates the radius of curvature of a wave front intersecting the beam axis at the coordinate z. The Gouy phase is $\varphi_{\rm G} = \tan^{-1}(z/z^r)$.

In the calculation process, we set the focus of the laser pulse as the origin, and electrons move toward the laser from $\{x_0,0,z_0\}$, where z_0 denotes a sufficiently far position, and x_0 denotes the initial off-axis position of the electron.

The momentum of the electron in an intense laser pulse can be determined by Lorentz and energy equations given below:

$$\frac{{\rm d}\boldsymbol{p}}{{\rm d}t} = -e\left(\boldsymbol{E}+\frac{\boldsymbol{u}}{c}\times\boldsymbol{B}\right), \tag{13}$$

$$\frac{{\rm d}\Gamma}{{\rm d}t} - e\left(\boldsymbol{v}\cdot\boldsymbol{E}\right). \tag{14}$$

Here, $\Gamma = \gamma mc^2$ represents the electron energy defined by the Lorentz factor $\gamma = [1-(v/c)^2]^{-1/2}$. $\boldsymbol{p} = \Gamma\boldsymbol{u}/c^2$, $\boldsymbol{v}$ is the electron velocity, and $\boldsymbol{u} = \boldsymbol{v}/c$. By solving the ordinary differential Eqs. (4)–(9) with Runge–Kutta method through MATLAB, the numerical solution of the electron's position, velocity, and acceleration are recorded for each step.

The electron dynamics can be explained using the ponderomotive potential model.[30] Lin *et al.*[31] suggested that for free electrons moving in a laser pulse, the mass force is the time average force experienced by the electron, that is, the low-frequency force generated by the high-frequency field:[31]

$$\boldsymbol{F}_{\rm Pond} = -\nabla V_{\rm Pond}(r,z,t), \tag{15}$$

where $V_{\rm Pond}$ is the ponderomotive potential and can be expressed as follows:

$$V_{\rm Pond} = \left(\sqrt{1+a^2/2}-1\right)mc^2. \tag{16}$$

Here, $a = eE/(mc)$ is the normalized amplitude of the electromagnetic field of the laser. As this paper is mainly a qualitative analysis, in order to simplify the calculation, the first-order approximation of the electric field is substituted into a to obtain

the first-order approximate direct proportion of the transverse and longitudinal ponderomotive forces:

$$F_{x\mathrm{Pond}} \propto \alpha_{x\mathrm{Pond}} = \frac{E_{\mathrm{L}}^2 \xi}{w^2\sqrt{1+E_{\mathrm{L}}^2/2}}, \tag{17}$$

$$F_{y\mathrm{Pond}} \propto \alpha_{y\mathrm{Pond}} = \frac{E_{\mathrm{L}}^2 \beta}{w^2\sqrt{1+E_{\mathrm{L}}^2/2}}, \tag{18}$$

$$F_{z\mathrm{Pond}} \propto \alpha_{z\mathrm{Pond}} = \frac{E_{\mathrm{L}}^2}{\sqrt{1+\frac{E_{\mathrm{L}}^2}{2}}}\left[\frac{2z\left(w^2-2\rho^2\right)}{w_0^2 w^4}+\frac{\eta}{L^2}\right]. \tag{19}$$

From knowledge of electrodynamics we know that the electron in relativistic acceleration emits electromagnetic radiation, and the radiated power per unit steradian angle can be expressed as follows:[32,33]

$$P_\Omega = \frac{\mathrm{d}P(t)}{\mathrm{d}\Omega} = \left[\frac{|\boldsymbol{n}\times[(\boldsymbol{n}-\boldsymbol{u})\times\boldsymbol{u}]|^2}{(1-\boldsymbol{n}\cdot\boldsymbol{u})^6}\right]_{t'}. \tag{20}$$

Here, the power radiated per unit solid angle P_Ω is normalized and the direction of radiation $\boldsymbol{n} = \{\sin(\theta)\cos(\phi), \sin(\theta)\sin(\phi), \cos(\theta)\}$, where θ represents the polar angle to the laser movement direction, and ϕ represents the azimuth angle on the plane perpendicular to origin point, $t = t' + R$, $R \sim R_0 - \boldsymbol{n}\cdot\boldsymbol{r}$, where t' is the time at which the electron interacts with the laser pulse, and R_0 denotes the distance from the origin to the observer, $\boldsymbol{r}$ is the position vector of the electron. The formula for the radiation energy per unit solid angle per unit frequency interval during the interaction of the electron with the laser pulse can be expressed using the following equation:[34,35]

$$\frac{\mathrm{d}^2 I}{\mathrm{d}\omega\mathrm{d}\Omega} = \left|\int_{-\infty}^{\infty}\frac{\boldsymbol{n}\times[(\boldsymbol{n}-\boldsymbol{u})\times\boldsymbol{u}]}{(1-\boldsymbol{n}\cdot\boldsymbol{u})^2}\mathrm{e}^{\mathrm{i}s(t-\boldsymbol{n}\cdot\boldsymbol{r})}\mathrm{d}t\right|^2, \tag{21}$$

where $\mathrm{d}^2 I/\mathrm{d}\omega\mathrm{d}\Omega$ is normalized using $e^2/(4\pi^2 c)$, $s = \omega_{\mathrm{s}}/\omega_0$, and ω_{s} is the frequency of the harmonic radiation. By solving Eqs. (20) and (21), the full time, full space and full spectral properties of the electron harmonic radiation can be obtained.

3. Numerical results

In our observations, we focused on radiation emitted from a sphere with a radius of 1 m, centered at the origin of the coordinates. The beam waist radius w_0 of the laser pulse is set to $2\lambda_0$, which corresponds to 2 μm, and the pulse duration L is 6.6 fs. The initial phase $\varphi_0 = 0$. The electron initially carries energy denoted by $\gamma = 5$ (equivalent to 2.56 MeV), moving in the direction opposite to the z-axis. This energy level can be achieved through acceleration via a linear accelerator. Given the characteristics of the circularly polarized laser pulse, the effects of the electron's off-axis collision with the laser pulse on the RNITS are modulated by the initial phase φ_0 of the laser pulse. Specifically, the impact on the electron from a pulse with an initial phase φ_0 at the radial off-axis angle α_0 is equivalent to the effect experienced by an electron subjected to a pulse with an initial phase $\varphi_0 + \alpha_1 - \alpha_0$ at the radial off-axis angle α_1. As such, the point of collision between the electron and the laser pulse, that is, the maximum value of the electron motion amplitude is positioned on the x-axis of the Cartesian coordinate system. For the purposes of our discussion, the radiated peak power per unit solid angle will be denoted as $\mathrm{d}p/\mathrm{d}\Omega$. It is important to note that all numerical results presented here are derived based on the physical laws and equations outlined in Section 2.

3.1. Electronic motion properties

As illustrated in Figs. 2(a)–2(d), with increasing laser pulse intensity, the final axial deviation extent of the off-axis electron's motion trajectory is more pronounced. Additionally, an electron with an initial off-axis position of $x_0 \neq 0$ deviates from the z-axis direction at a constant speed after the primary interaction stage with the laser pulse. The final deviation speed is closely tied to the intensity of the laser pulse, as depicted in Figs. 2(e)–2(h).

This phenomenon can be attributed to the fact that, when the electron centrally collides with the laser pulse, the transverse ponderomotive force experienced by the electron at each directional angle is equal over a macroscopic time scale. As a result, the electron follows a circular-like spiral motion, observable in Figs. 2(a)–2(d).

When an electron moves off-axis, it is subjected to a slight decay of the transverse ponderomotive force in the off-axis direction, along with a relatively larger ponderomotive force in other directions. This can be seen in Figs. 2(i)–2(l). In extreme cases (e.g., $a_0 = 10$ as shown in Fig. 2(l)), the ponderomotive force experienced by the electrons becomes highly irregular. This irregularity in force induces a change in the trajectory and transverse velocity of the electron's motion. As the laser intensity increases, so too does the transverse ponderomotive force on the electron, amplifying the aforementioned effects. Consequently, the degree of axial deviation of the electron with respect to its initial off-axis position naturally escalates.

Moreover, it is noteworthy from Figs. 2(a)–2(d) that the final axial deviation angle of the electron's trajectory does not have a direct correlation with the electron's initial off-axis position x_0. Specifically, when the $a_0 < 10$, the final axial deviation angle of the electron's trajectory is at its maximum when the initial off-axis position $x_0 = 1\lambda_0$. However, when $a_0 = 10$, the maximum final axial deviation angle of the trajectory occurs when the initial off-axis position of the electron $x_0 = 0.5\lambda_0$.

This phenomenon can be attributed to the limitation of the laser pulse's beam waist on the effective transverse ponderomotive action of the laser pulse on the off-axis electron. In this

study, the beam waist radius of the laser pulse $b_0 = 2\lambda_0$. The ponderomotive force's impact on the electron in the longitudinal direction is significantly smaller than that in the transverse direction, as depicted in Figs. 2(i)–2(p). Hence, the electron's longitudinal motion speed is primarily influenced by its initial energy.

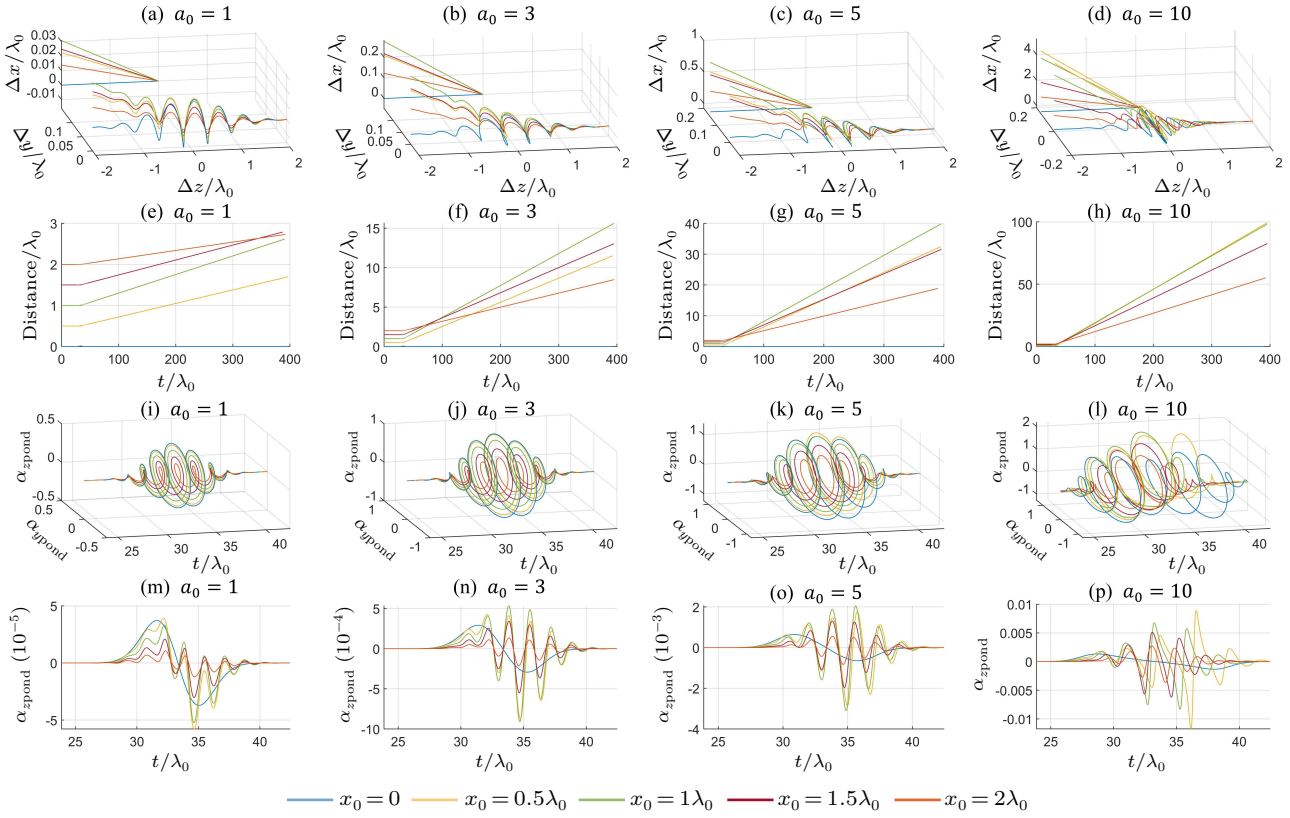


Fig. 2. Effect of the electron's initial off-axis position x_0 on the electron trajectories under the action of laser pulses with different laser peak amplitudes a_0, where (a)–(d) illustrate the longitudinal changes of the electron motion compared to the initial position, along with the projection deviation angle (the connection between the origin and the point $z \leq -100\lambda_0$), and (e)–(h) represent the distances of the electrons from the center axis of the laser pulse at different moments. (i)–(l) represent the transversal ponderomotive factors (the term after the proportional sign in Eqs. (17) and (18)), (m)–(p) represent the longitudinal ponderomotive factors (the term after the proportional sign in Eq. (19)).

Indeed, this study primarily conducts a qualitative analysis of the ponderomotive force, and the results shown in Figs. 2(i)–2(p) represent the first-order approximate direct proportional quantities $\alpha_{x\text{Pond}}$, $\alpha_{y\text{Pond}}$ and $\alpha_{z\text{Pond}}$ in Eqs. (14)–(16). These can be interpreted as normalized first-order approximations of the ponderomotive force. This approach allows us to compare the magnitudes of the ponderomotive forces experienced by electrons under different conditions.

The degree of transverse deviation of the electron can be characterized by the following two measures:

(i) The ratio of the transverse ponderomotive force exerted on the electron in the off-axis direction to that in the on-axis direction.

(ii) The magnitude of the total transverse ponderomotive force applied to the electron.

As can be observed from Figs. 2(i)–2(l), the first aspect demonstrates a positive correlation with the electron's initial off-axis position x_0, while the latter shows a negative correlation with the same. This contrasting behavior creates a situation where the electron's initial off-axis position x_0 does not exhibit a straightforward positive or negative correlation with the final axial deviation of the electron's trajectory. Instead, this relationship is significantly influenced by the intensity of the laser pulse.

3.2. Electron space relativistic nonlinear Thomson inverse scattering properties

3.2.1. Peak power properties of electron space radiation

It is readily apparent from Figs. 3(a) and 3(b) that when the intensity of the laser pulse is relatively low ($a_0 \leq 3$), the angular distribution of the electron radiation power displays an annular shape with a hollow center. This finding aligns with Taira *et al.*'s[19] studies of higher harmonics.

In this study, the beam waist radius of the laser pulse, $b_0 = 2\lambda_0$, placing it in the category of highly tightly focused laser pulses. The action of the transverse ponderomotive force of the laser field is tightly confined to a relatively close distance from the laser pulse axis. Additionally, the electron under examination does not fall into the category of high-energy particles, as it has a relatively low longitudinal velocity compared to high-energy electrons. This results in the laser field's

period of action being relatively long, which means that the overall action of the transverse ponderomotive force on the electron is considerably higher than that applied to ultra-high-energy electrons in a plane wave laser field. Consequently, the divergence of its radiation, or the angular distribution of the first harmonic peak of the radiation, is quite distinct from the distribution of higher harmonics in the plane wave laser field, as studied by Taira *et al.*[19]

As shown in Figs. 2(i)–2(l), when the laser pulse peak amplitude $a_0 \leq 5$, the longer the electron's initial off-axis position x_0, the lower the transverse ponderomotive force experienced by the electron, and the better the collimation of the electron's spatial radiation. This is evident even when $x_0 = 2.8\lambda_0$ as shown in Fig. 3(a), where the annular shape distribution of the electron radiation power disappears and reverts to a single peaked distribution. However, as the laser pulse intensity increases, the collimation of the electron's spatial radiation deteriorates and the asymmetry of the radiation becomes increasingly pronounced for the same x_0.

As shown in Figs. 4(a) and 4(b), when the peak amplitude of the light pulse $a_0 \geq 5$, and the initial off-axis position of the electron $x_0 < 1\lambda_0$, the spatial radiation collimation of off-axis electrons is weaker than when the initial position of the electron is on the central axis of the laser pulse. This indicates that, under the influence of a strong laser pulse, the spatial radiation collimation of the electron is not positively correlated with the initial off-axis position of the electron, x_0. The explanation for this phenomenon will be discussed subsequently.

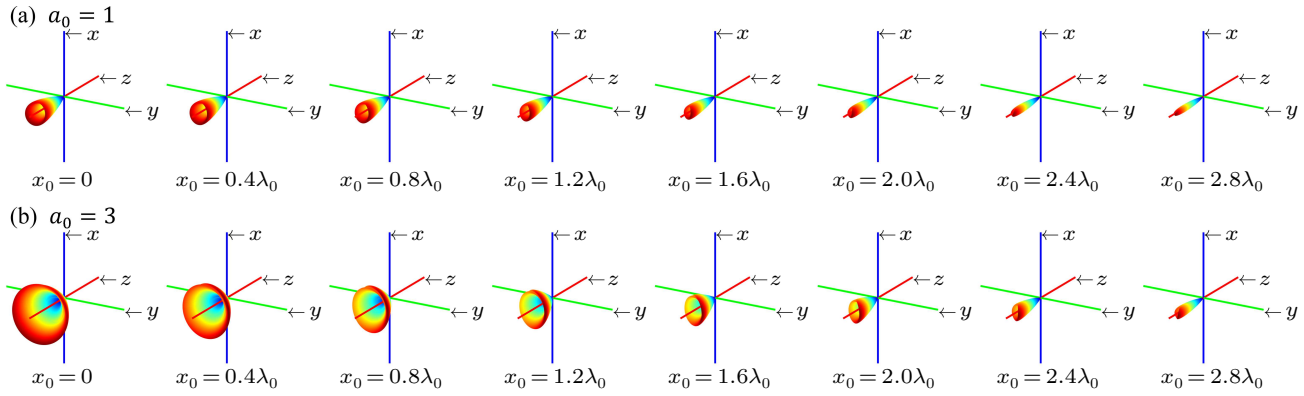


Fig. 3. Effect of the distance x_0 of the electron initial position collision from the central axis of the laser pulse on the maximum power distribution per unit angle of spatial radiation under the action of relatively low laser pulses ($a_0 = 1$ (a) and $a_0 = 3$ (b)).

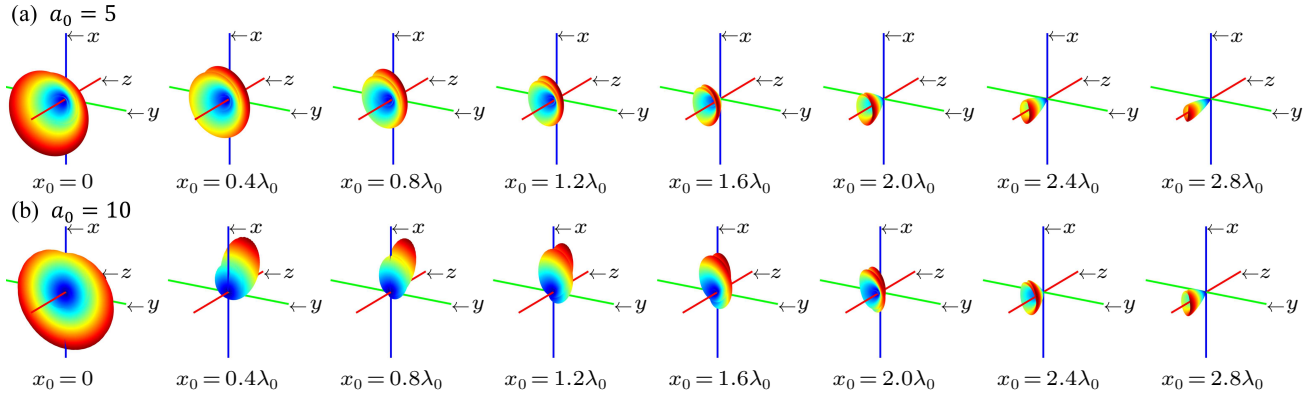


Fig. 4. Effect of the distance x_0 of the electron initial position collision from the central axis of the laser pulse on the maximum power distribution per unit angle of spatial radiation under the action of relatively high laser pulses ($a_0 = 5$ (a) and $a_0 = 10$ (b)).

When the laser pulse intensity surpasses the relativistic intensity, the spatial radiation symmetry of the electron breaks as the initial off-axis position x_0 increases, exhibiting a vortex state for the first time in the collision scenario. This occurs due to the instability of the transverse ponderomotive force acting on the electron during off-axis motion, which leads to an unstable transverse drift motion. The radius of curvature frequently changes in the strong laser field, which subsequently causes significant alterations to the electron's spatial radiation and disrupts the symmetry of the power distribution.

When the initial off-axis position x_0 of the electron exceeds the beam waist radius of the laser pulse, the transverse ponderomotive force acting on the electron becomes too small. Consequently, the unstable transverse drift motion is no longer as pronounced compared to the longitudinal motion, and the instability of the electron's transverse angular radiation weakens. This results in the disappearance of its vortex state and an improvement in collimation.

When the laser pulse peak amplitude $a_0 = 10$ and the initial off-axis position x_0 just begins to deviate from the central

axis of the laser pulse, the primary radiation direction of the electron surprisingly shifts to the forward direction. This implies that the lateral drift motion of the electron is highly unstable in an ultra-intense laser field ($a_0 \geq 10$), and the asymmetry exacerbates to the extent that it alters the basic characteristic of backward radiation. Therefore, in practical experiments, when the peak amplitude of the laser pulse $a_0 \geq 10$, researchers must consider observing the spatial radiation of off-axis electrons from the forward direction. Failing to do so may lead to incorrect conclusions regarding the angular power of the radiation unit.

Next, we delve deeper into the instantaneous maximum power represented by $\max(\mathrm{d}p/\mathrm{d}\Omega)$ and the off-axis angle θ_0 at the extreme value of the electron's spatial radiation. These parameters respectively reflect the instantaneous maximum power of the electron's spatial radiation and the collimation of the radiation, both of which are crucial for experimental purposes. Figures 5(a) and 5(b) depict the relationships between these parameters and the laser intensity as well as the initial off-axis position of the electron.

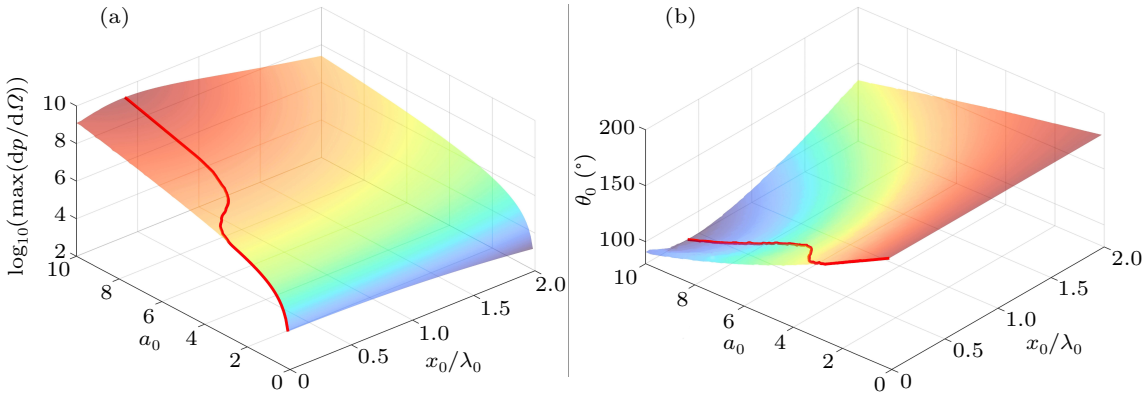


Fig. 5. Effect of the distance x_0 of the initial position of the electron collision off the central axis of the laser pulse on the logarithmic value of the peak unit angular power of radiation $\log_{10}[\max(\mathrm{d}p/\mathrm{d}\Omega)]$ (a) and the peak angle of radiation θ_0 (b) under the action of laser pulses with different peak amplitudes a_0, where the red lines mark the initial off-axis position x_0 and value corresponding to the maximum peak radiation (a) and the minimum peak angle of radiation (b), respectively, under the same a_0 condition.

One key point to note is that as the laser pulse intensity intensifies, the relationship between the peak power magnitude of the electron's spatial radiation and the electron's initial off-axis position, x_0, shifts from being negatively correlated to first increasing and then decreasing. This suggests that the maximum power radiation of the electron under the influence of a high-energy laser pulse is not associated with an on-axis collision, but instead with an off-axis collision.

The explanation for this phenomenon can be drawn from the discussion about the ponderomotive force on off-axis electrons in Subsection 3.1. When the laser pulse is relatively weak ($a_0 < 5$ in this case, but more specifically $a_0 < 4.5$), the transverse ponderomotive force of the laser pulse is rather small, as shown in Figs. 2(i) and 2(j). Given the electron's high longitudinal velocity, the impact of the asymmetric ponderomotive force on its motion is relatively weak. As the electron strays further and further from the laser pulse's central axis, its transverse ponderomotive force decreases, leading to a corresponding reduction in the power of the electron's excited radiation.

When the laser pulse is relatively intense ($a_0 > 4.5$), as studied in this paper), the asymmetry of the ponderomotive force on the electron moving off-axis cannot be ignored. As illustrated in Figs. 2(k) and 2(l), the magnitude of the ponderomotive force in the off-axis direction is greater than that in the direction opposite to the off-axis. Consequently, over the macroscopic time scale, the electron experiences an additional net ponderomotive force in the off-axis direction. The ratio of this force to the combined ponderomotive force rises with an increase in x_0.

However, due to the constraints of the laser beam waist, the combined ponderomotive force diminishes as x_0 increases. Under the combined effect of both the ratio and combined force, when the initial off-axis position x_0 is relatively small but $x_0 \neq 0$, the net effect of the combined transverse ponderomotive force over the macroscopic time scale still exhibits an increasing trend as x_0 gradually increases. This is despite the rising transverse asymmetric ponderomotive force ratio and the declining combined ponderomotive force.

As x_0 increases further, the net effect of the combined transverse ponderomotive force over the macroscopic time scale diminishes due to the even faster decline of the transverse ponderomotive force from all directions. Although the ratio of the transverse asymmetric ponderomotive force on the electron continues to increase, it cannot compensate for the drastic decrease in the overall ponderomotive force. This results in a decline in the net combined transverse ponderomotive force, which in turn leads to a decrease in the peak power radiated from the electron in space.

Additionally, a detailed examination of Fig. 5(b) reveals that the numerical distribution in Figs. 5(b) and 5(a) exhibits clear symmetry. Even the distribution of the extreme point

within the unit laser peak amplitude is the same, which means that the patterns in these two aspects correspond to each other.

As the intensity of the laser pulse increases, the relationship between the peak power angle of the electron's spatial radiation and the electron's initial off-axis position x_0 gradually transitions from a positive correlation to a pattern that first decreases and then increases. This implies that the collimation of the electron's spatial radiation is negatively correlated with the magnitude of the maximum power under identical initial electron energy, laser pulse width, and beam waist radius conditions. This means we cannot achieve electron radiation with both high collimation and high power simultaneously by simply modifying the laser pulse intensity and the initial off-axis position of the electron. The explanation for this can be found by considering electron dynamics. The electron, subjected to the action of the transverse ponderomotive force, undergoes energy changes and subsequently generates radiation. The power magnitude of the radiation is positively correlated with the degree of action of the transverse ponderomotive force. However, the action of the transverse ponderomotive force also leads to instability in the electron's transverse drift. Therefore, under the same basic conditions of initial electron energy, laser pulse width, and beam waist radius, the collimation of the electron's spatial radiation and its power magnitude are mutually exclusive.

3.2.2. Spectral properties of electron radiation

The deviation of the electron radiation spectrum from the symmetry axis of the laser pulse, along with its light intensity and harmonic frequency characteristics, were assessed. The results are presented in Figs. 6 and 7.

Figures 6(a) and 6(b) clearly shows that at relatively low laser intensities ($a_0 < 5$), the spatial radiation spectrum of the electron gravitates toward the central axis of the laser pulse as the initial off-axis position x_0 increases. This suggests a strengthening of the collimation of the electron's spatial radiation spectrum. Simultaneously, as the initial off-axis position x_0 of the electron increases, the harmonic peak of the electron radiation spectrum starts to red-shift. The wave number is gradually increasing, and the harmonic light intensity of the spectrum also diminishes.

This behavior arises from the relatively low joint transverse ponderomotive force acting on the off-axis electron in low-intensity laser fields. As the initial off-axis distance of the electron increases, the transverse ponderomotive force decreases, resulting in a reduction of the transverse drift motion. Consequently, the collimation of the electron spectrum improves, and the harmonic light intensity decreases.

Moving on to Figs. 7(a) and 7(b), we observe that in the case of relatively strong laser pulses, similar to the spatial radiation properties discussed earlier, the radiation spectral properties of the electron change with an increase in the initial off-axis position x_0. Initially, the spectrum shifts toward higher frequencies and energies, becomes multimodal, and subsequently transitions to a state of under-collimation, lower frequencies, lower energies, and super-continuum generation with higher collimation.

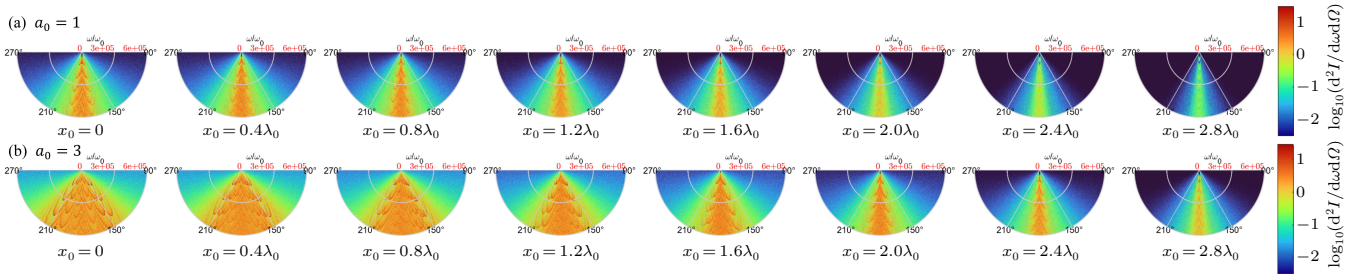


Fig. 6. Spatial radiation spectrum θ angle distribution when the distance x_0 of the electron's initial position of the collision deviates from the center axis of the laser pulse varies under the action of relatively low laser pulses ($a_0 = 1$ (a) and $a_0 = 3$ (b)).

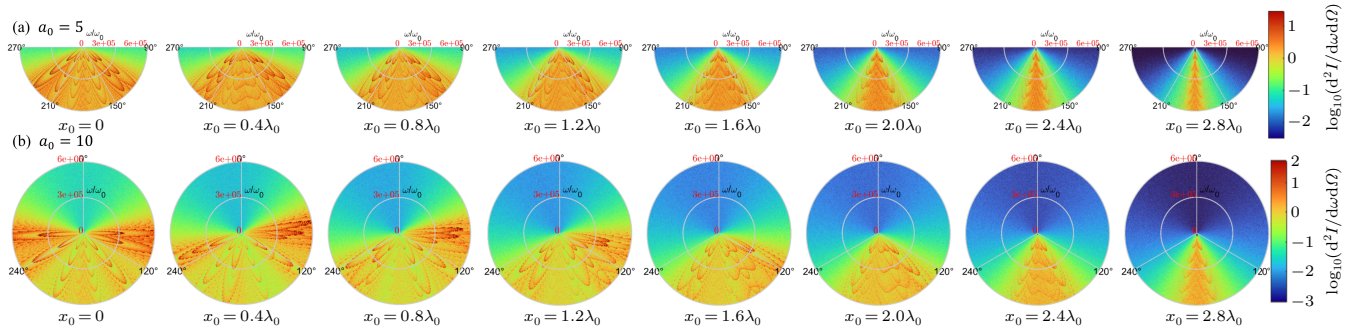


Fig. 7. Spatial radiation spectrum θ angle distribution when the distance x_0 of the electron's initial position of the collision deviates from the center axis of the laser pulse varies under the action of relatively high laser pulses ($a_0 = 5$ (a) and $a_0 = 10$ (b)).

In particular, when the laser peak amplitude $a_0 = 10$, the first harmonic peak of the electron at an initial off-axis position $x_0 = 2.4\lambda_0$ (with an observed θ angle of approximately 80°) can reach a frequency of 1.8×10^{20} Hz. This frequency range corresponds to high-frequency gamma rays and holds potential for applications in cancer treatment through radiation therapy. Subsequently, as x_0 increases further, the first harmonic peak of the electron radiation starts to red-shift. For $x_0 \geq 2.4\lambda_0$, the first harmonic peak no longer falls within the range of gamma rays, but rather within the range of x-rays.

At the electron's initial off-axis position $x_0 = 2.8\lambda_0$, the collimation of the radiation spectrum is notably enhanced compared to when the electron is closer to the axis. The peak harmonic distribution of the radiation is concentrated within the range of $180° \pm 15°$. Additionally, the attenuation of the intensity in the above electron radiation spectrum is considerably limited within this harmonic distribution range due to the superposition of interference between the harmonics.

Based on the observations from Figs. 6 and 7, we can draw the following conclusion: when the laser pulse peak amplitude a_0 is relatively low, the electron radiation spectrum exhibits a noticeable axial symmetry with respect to the laser pulse axis. However, as the laser pulse peak amplitude a_0 increases, this axial symmetry is broken, resulting in an asymmetric frequency distribution of the first harmonic peak even with a small increase in the initial off-axis position x_0. Specifically, the harmonic peak shows a blue-shifted trend in the $X+$ direction and a red-shifted trend in the $X-$ direction. As x_0 continues to increase, the collimation of the electron radiation improves, leading to red-shifted harmonic peaks and a restoration of symmetry in the electron radiation spectrum about the laser pulse axis.

Furthermore, the convergence of electron radiation harmonics toward the central axis of the laser pulse is evident in Figs. 6 and 7. As this convergence occurs, the multimodal nature of the radiation spectrum diminishes, giving way to significant interference superposition between the harmonics. This results in the electron radiation harmonics displaying distinct super-continuum spectral properties. This effect is particularly prominent when the initial off-axis position of the electrons is beyond the waist of the laser pulse beam, that is, when $x_0 > 2\lambda_0$.

Our analysis included measurements of the radial distribution, light intensity, and harmonic frequency properties of the electron radiation spectrum, as depicted in Figs. 8 and 9.

From Figs. 8(a) and 8(b) it is evident that the radial distribution of the electron radiation exhibits significant symmetry around $\phi = 0°$ in the case of a low-intensity laser field. This symmetry arises due to the relatively small transverse ponderomotive force acting on the electrons and the resulting weak influence of transverse drift motion, which leads to pronounced transverse symmetry.

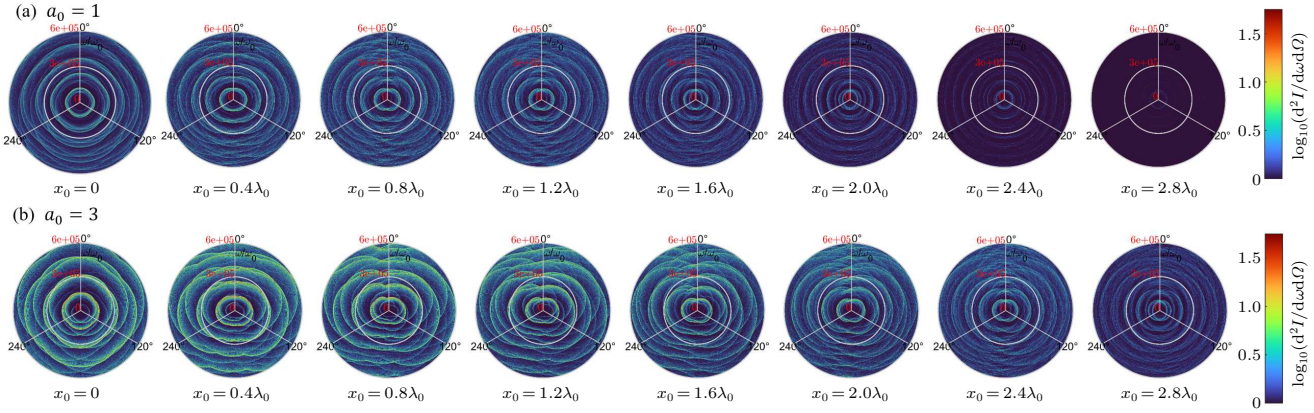


Fig. 8. Angular distribution of the spatial radiation spectrum ϕ for the variation of the distance x_0 from the central axis of the laser pulse at the initial position of the electron collision under the action of the laser pulse with relatively low peak amplitude ($a_0 = 1$ (a), $a_0 = 3$ (b)).

Furthermore, when the laser pulse intensity is relatively low, the harmonic peaks near $\phi = 0°$ and $\phi = 180°$ exhibit a red-shift as the initial off-axis position x_0 of the electron increases. However, there is no significant frequency change observed in the harmonic peaks near $\phi = 90°$ and $\phi = 270°$. Additionally, the intensity of the radiation spectrum decreases as the initial off-axis position x_0 of the electron increases. The explanation for this behavior has been previously discussed and is not reiterated here.

However, when the off-axis electron is subjected to an intense laser pulse, as shown in Figs. 9(a) and 9(b), the radial distribution of the radiation spectrum loses its symmetry. The distribution of harmonic peaks becomes concentrated in the range $\phi \in (-90°, 90°)$, with a significant decrease in harmonic light intensity near $\phi = 180°$. The explanation for this phenomenon can be linked to the earlier discussion in Figs. 7(a) and 7(b), where it was observed that the harmonic peaks experience a blue-shift followed by a red-shift as the initial off-axis position x_0 of the electron increases. Additionally, due to the asymmetry of the ponderomotive force exerted by the intense

laser pulse, the electron undergoes unstable transverse drift motion. This instability contributes to the loss of symmetry in the radiation spectrum distribution, with dominance from the direction of transverse drift motion. However, as the initial position of the electron moves further away from the central axis of the laser pulse, the unstable transverse drift motion weakens, resulting in a restoration of symmetry in the distribution of the electron's spatial radiation spectrum.

In addition, figures 9(a) and 9(b) reveal that in the strong laser field, the off-axis electron radiation spectrum exhibits two main radiation directions. These directions are characterized by the main harmonic direction angles: $\phi_{\text{main}} \in (-90^\circ, 0^\circ)$, which are called referred to as $Y-$ direction harmonics, and $\phi_{\text{main}} \in (0^\circ, 90^\circ)$, referred to as $Y+$ direction harmonics in this paper. When the laser pulse peak amplitude $a_0 < 10$, the harmonic peaks of the electron radiation are distributed around $\phi = 0^\circ$ due to the interference superposition of the $Y-$ and $Y+$ direction harmonics. However, when the laser pulse peak amplitude $a_0 = 10$, the multimodality of the electron radiation spectrum becomes significantly enhanced. As a result, the $Y-$ and $Y+$ direction harmonics no longer appear in interference superposition, leading to a different distribution of the harmonic peaks in the electron radiation spectrum away from $\phi = 0^\circ$.

In addition, in Figs. 9(a) and 9(b), the $Y-$ direction harmonics of the off-axis electron generally exhibit higher frequencies compared to the $Y+$ direction harmonics. Furthermore, as the initial off-axis distance x_0 increases, the frequency difference between the $Y-$ and $Y+$ direction harmonics gradually decreases. This indicates that the red-shift and blue-shift effects on the $Y-$ direction harmonics with changes in the initial off-axis distance x_0 are more pronounced compared to the frequency changes observed in the $Y+$ direction harmonics.

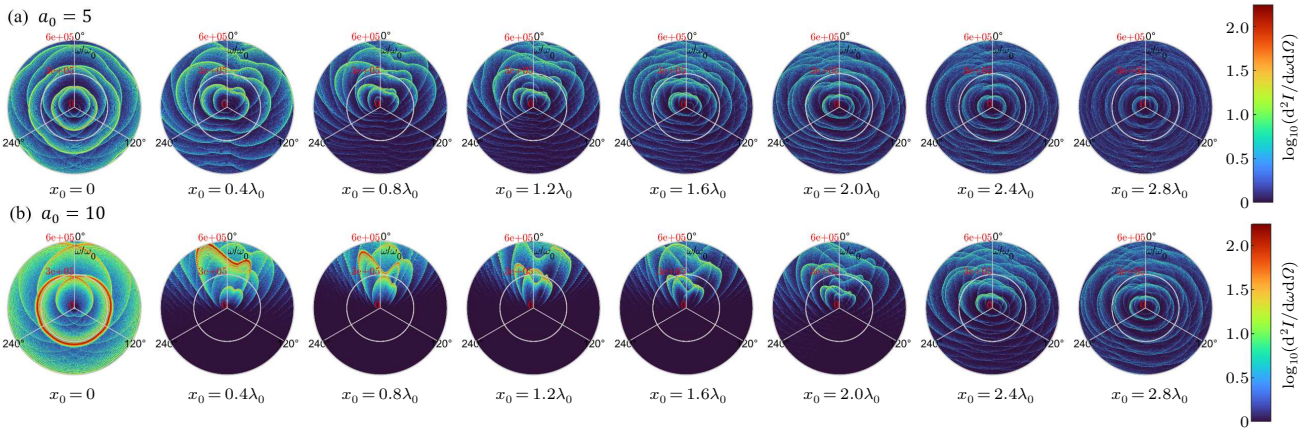


Fig. 9. Angular distribution of the spatial radiation spectrum ϕ for the variation of the distance x_0 from the central axis of the laser pulse at the initial position of the electron collision under the action of the laser pulse with relatively high laser pulses ($a_0 = 5$ (a) and $a_0 = 10$ (b)).

4. Conclusion and perspectives

In this study, we have investigated the variations in electron dynamics, radiated power, and spectral properties in RNTIS. Specifically, we focused on the collisions between tightly focused circular polarized lasers and electrons considering the influence of laser intensity and the initial off-axis position of the electrons. From the perspective of electron dynamics, we observed that off-axis electrons experience deviations from axial motion due to the combined effect of the transverse ponderomotive force. The magnitude of the deviation angle and speed is influenced by the initial off-axis position of the electrons and the peak amplitude of the laser pulse.

At relatively low laser pulse intensities ($a_0 < 4.5$), we observed a monotonic variation in electron radiation properties with the initial off-axis position of the electron. The angular distribution of the spatially radiated power decreases as the initial off-axis distance of the electron x_0 increases, indicating an enhancement in collimation. The multimodality of the electron radiation spectrum weakens, and a phenomenon of super-continuous spectrum appears. Additionally, the harmonic peaks of the radiation spectrum are red-shifted, resulting in a decrease in radiation intensity. Notably, the radiation radial direction exhibits significant symmetry about $\phi = 0^\circ$.

At relatively high laser pulse intensities ($a_0 > 4.5$), the electron spatial radiation properties exhibit a distinct variation with the initial off-axis position of the electron. This variation is attributed to the transverse asymmetric ponderomotive force acting on the electron. The spatial radiation power angle distribution of the electron initially increases and then decreases as x_0 increases, while the collimation first decreases and then increases. Interestingly, the value of x_0 corresponding to the highest peak radiation power is the same as the value of x_0 corresponding to the lowest peak radiation angle for a given laser pulse intensity. The multimodal nature of the electron radiation spectrum behaves differently in different directions as x_0 varies, and the radiation spectrum exhibits a blue-shift phenomenon in specific directions. Furthermore, as x_0 further increases, the radiation spectrum harmonic peaks experience a

red-shift phenomenon in all directions.

In summary, to obtain high-energy, highly monochromatic, and high-frequency gamma rays within certain parameters such as the laser pulse beam radius, pulse width, and electron initial energy, the laser pulse intensity can be increased. When $a_0 > 4.5$, it is possible to deliberately deviate the electron from the central axis of the laser during the initial phase. However, this results in relatively weak collimation of the electron radiation. On the contrary, if high collimation of the electron radiation is desired, the initial off-axis position of the electron can be significantly increased, while simultaneously reducing the laser pulse intensity. However, this approach leads to lower power, weaker monochromaticity, and lower frequency of the electron radiation. These findings provide a valuable method for utilizing RNITS as a radiation source for scientific experiments and applications, including cancer treatment. By optimizing the laser pulse intensity and the initial off-axis position of the electron, researchers can strike a balance between power, collimation, monochromaticity, and frequency to meet their specific requirements.

Acknowledgments

Project supported by the National Natural Science Foundation of China (Grant Nos. 10947170/A05 and 11104291), the Natural Science Fund for Colleges and Universities in Jiangsu Province (Grant No. 10KJB140006), the Natural Sciences Foundation of Shanghai (Grant No. 11ZR1441300), and the Natural Science Foundation of Nanjing University of Posts and Telecommunications (Grant No. NY221098). We also thank the Jiangsu Qing Lan Project for their sponsorship.

References

[1] Li Y T, Wang W M, Li C and Sheng Z M 2012 *Chin. Phys. B* **21** 095203
[2] Wang M X, Chen S G, Liang H and Peng L Y 2020 *Chin. Phys. B* **29** 013302
[3] Xue Y H, He B, Zhou J, Li Z, Fan Y Y, Qi Y F, Liu C, Yuan Z J, Zhang H B and Lou Q H 2011 *Chin. Phys. Lett.* **28** 054212
[4] Guo Y, Liu A, Wang J and Liu X 2019 *Chin. Phys. B* **28** 094212
[5] Sheng Z M, Weng S M, Yu L L, Wang W M, Cui Y Q, Chen M and Zhang J 2015 *Chin. Phys. B* **24** 015201
[6] Kong W J, Shen Z C, Wang S H, Shao J D, Fan Z X and Lu C J 2010 *Chin. Phys. B* **19** 044210
[7] Inada T, Yamazaki T, Yamaji T, Seino Y, Fan X, Kamioka S, Namba T and Asai S 2017 *Appl. Sci.* **7** 671
[8] Mourou G A, Tajima T and Bulanov S V 2006 *Rev. Mod. Phys.* **78** 309
[9] Strickland D 2019 *Rev. Mod. Phys.* **91** 030502
[10] Schlenvoigt H P, Heinzl T, Schramm U, Cowan T E and Sauerbrey R 2016 *Phys. Scripta* **91** 023010
[11] Zhuang J, Yan Y, Zhou X, Chen Z, Ren S and Tian Y 2021 *Laser Phys.* **31** 035401
[12] Pogorelsky I, Polyanskiy M and Shaftan T 2020 *Phys. Rev. Accel. Beams* **23** 120702
[13] Jiang Y J, Liang Y Y, Gao Y T, Zhao K, Xu S Y, Wang J, He X K, Teng H, Zhu J F and Chen Y L 2020 *Chin. Phys. B* **29** 013206
[14] Yan W, Fruhling C, Golovin G, Haden D, Luo J, Zhang P, Zhao B, Zhang J, Liu C and Chen M 2017 *Nat. Photonics* **11** 514
[15] Taira Y and Katoh M 2018 *Phys. Rev. A* **98** 052130
[16] Artyukov I, Dyachkov N, Feshchenko R, Polunina A, Popov N, Shvedunov V and Vinogradov A 2017 *Proc. X ray Lasers and Coherent X ray Sources: Development and Applications*, April 24–26, 2017 Prague, Czech Republic p. 7
[17] Chi Z, Du Y, Yan L, Zhang H, Huang W and Tang C 2022 *Proc. 8th Symp. on Novel Photoelectronic Detection Technology and Applications*, November 9–11, 2022 Kunming, China, p. 297
[18] Vanacore G M, Madan I, Berruto G, Wang K, Pomarico E, Lamb R, Mcgrouther D, Kaminer I, Barwick B and García De Abajo F J 2018 *Nat. Commun.* **9** 2694
[19] Zhang Y, Wang M, Ning Z, Cao E, Liu X and Nie Z 2022 *Opt. Laser Technol.* **149** 107844
[20] Datte P, Ross J, Froula D, Daub K, Galbraith J, Glenzer S, Hatch B, Katz J, Kilkenny J and Landen O 2016 *Rev. Sci. Instrum.* **87** 11E549
[21] Taira Y, Hayakawa T and Katoh M 2017 *Sci. Rep.* **7** 5018
[22] Taira Y and Katoh M 2018 *Astrophys. J.* **860** 45
[23] Liu C, Kohler M C, Hatsagortsyan K Z, Müller C and Keitel C H 2009 *New J. Phys.* **11** 105045
[24] Chang Y, Zeng Z, Wang C, Long Z and Tian Y 2022 *Appl. Opt.* **61** 6038
[25] Yu W, Yu M, Ma J, Sheng Z, Zhang J, Daido H, Liu S, Xu Z and Li R 2000 *Phys. Rev. E* **61** R2220
[26] Barton J P and Alexander D R 1989 *J. Appl. Phys.* **66** 2800
[27] Yariv A 1989 *Quantum electronics* (New York: John Wiley & Sons) pp. 123
[28] Salamin Y I and Keitel C H 2002 *Phys. Rev. Lett.* **88** 095005
[29] Zhang S 2010 *J. At. Mol. Sci.* **1** 308
[30] Kibble T 1966 *Phys. Rev.* **150** 1060
[31] Lin D, Kong Q, Chen Z, Wang P and Ho Y 2008 *J. Phys. D: Appl. Phys.* **41** 135107
[32] He F, Lau Y, Umstadter D P and Kowalczyk R 2003 *Phys. Rev. Lett.* **90** 055002
[33] He F, Yu W, Lu P, Xu H, Qian L, Shen B, Yuan X, Li R and Xu Z 2003 *Phys. Rev. E* **68** 046407
[34] Gao J 2004 *Phys. Rev. Lett.* **93** 243001
[35] Cao W, Lan P F and Lu P X 2006 *Acta Phys. Sin.* **55** 2115 (in Chinese)